

Lactobacillus fermentum CECT5716: a novel alternative for the prevention of vascular disorders in a mouse model of systemic lupus erythematosus

Marta Toral,* Iñaki Robles-Vera,* Miguel Romero,*[†] Néstor de la Visitación,* Manuel Sánchez,*[†] Francisco O'Valle,^{†,‡} Alba Rodríguez-Nogales,*[†] Julio Gálvez,*^{†,§,¶} Juan Duarte,*^{†,¶,||,1} and Rosario Jiménez*^{†,||}

*Department of Pharmacology, School of Pharmacy, [†]Department of Pathology, School of Medicine, [§]Centro de Investigación Biomedica en Red de Enfermedades Hepáticas y Digestivas (CIBER-EHD), and [¶]Center for Biomedical Research (CIBM), University of Granada, Granada, Spain; [†]Instituto de Investigación Biosanitaria de Granada (Ibs.GRANADA), Granada, Spain; and ^{||}Centro de Investigación Biomédica en Red Enfermedades Cardiovasculares (CIBERCV), Granada, Spain

ABSTRACT: The aim of the present study was to examine whether the immune-modulatory bacteria *Lactobacillus fermentum* CECT5716 (LC40) ameliorates disease activity and cardiovascular complications in a female mouse model of lupus. Eighteen-week-old NZBWF1 [systemic lupus erythematosus (SLE)] and NZW/LacJ (control) mice were treated with vehicle or LC40 (5×10^8 colony-forming units/d) for 15 wk. LC40 treatment reduced lupus disease activity, blood pressure, cardiac and renal hypertrophy, and splenomegaly in SLE mice. LC40 reduced the elevated T, B, regulatory T cells (T_{reg}), and T helper (T_H)-1 cells in mesenteric lymph nodes of lupus mice. LC40 lowered the higher plasma concentration of proinflammatory cytokines observed in lupus mice. Aortas from SLE mice showed reduced endothelium-dependent vasodilator responses to acetylcholine. Endothelial dysfunction found in SLE is related to an increase of both NADPH oxidase-driven superoxide production and eNOS phosphorylation at the inhibitory Thr⁴⁹⁵. These activities returned to normal values after a treatment with LC40. Probiotic administration to SLE mice reduced plasma LPS levels, which might be related to an improvement of the gut barrier integrity. LC40 treatment increases the *Bifidobacterium* count in gut microbiota of SLE mice. In conclusion, our findings identify the gut microbiota manipulation with LC40 as an alternative approach to the prevention of SLE and its associated vascular damage.—Torral, M., Robles-Vera, I., Romero, M., de la Visitación, N., Sánchez, M., O'Valle, F., Rodríguez-Nogales, A., Gálvez, J., Duarte, J., Jiménez, R. *Lactobacillus fermentum* CECT5716: a novel alternative for the prevention of vascular disorders in a mouse model of systemic lupus erythematosus. FASEB J. 33, 10005–10018 (2019). www.fasebj.org

KEY WORDS: hypertension · endothelial dysfunction · oxidative stress · gut dysbiosis · probiotics

Systemic lupus erythematosus (SLE) is one of the most deleterious autoimmune inflammatory diseases. SLE is related to an increased risk of renal and cardiovascular

disease development (1), the most important cause of mortality in SLE patients (2). This disease is associated with a high incidence of hypertension (3). Nevertheless, the pathophysiological mechanisms promoting SLE hypertension have been poorly explored. Several studies suggest that oxidative stress is important in the pathogenesis of hypertension in SLE (4). The immune system is involved in the development of vascular inflammation, and oxidative stress is linked to hypertension (5). However, whether immune cells contribute to endothelial dysfunction and hypertension in SLE is largely unknown.

Gut microbiota might trigger symptoms and progression of some autoimmune diseases (6). A disbalance in gut microbiota populations in SLE patients was described, characterized by a significantly lower Firmicutes/Bacteroidetes (F/B) ratio (6, 7), a lower diversity of gut microbiota, and changes in several bacterial species, in particular, an increased representation of Gram-negative

ABBREVIATIONS: anti-dsDNA, anti-double-stranded DNA; BP, blood pressure; CFU, colony-forming unit; DHE, dihydroethidium; F/B, Firmicutes/Bacteroidetes; HEPES, 4-(2-hydroxyethyl)-1-piperazineethanesulfonic acid; HR, heart rate; IAP, intestinal alkaline phosphatase; LC40, *Lactobacillus fermentum* CECT5716; L-NAME, N^G-nitro-L-arginine methyl ester; LDA, linear discriminant analysis; *lpr*, lupus-prone MRL/Mp-Fas; MRL, Murphy Roths Large; NOX, NADPH oxidase; OTU, operational taxonomy unit; QIIME, Quantitative Insights Into Microbial Ecology; RhoA, Ras homolog gene family, member A; ROS, reactive oxygen species; SBP, systolic BP; SLE, systemic lupus erythematosus; SNP, sodium nitroprusside; T_H , T helper; T_{reg} , regulatory T cell

¹ Correspondence: Department of Pharmacology, School of Pharmacy, University of Granada, Campus de Cartuja s/n, 18071 Granada, Spain. E-mail: jmduarte@ugr.es

doi: 10.1096/fj.201900545RR

This article includes supplemental data. Please visit <http://www.fasebj.org> to obtain this information.

bacteria consistent with an increased serum level of LPS (8). In lupus-prone Murphy Roths Large (MLR)/Mp-Fas lpr (lpr) mice, it has been described that the dynamics of microbiota play a critical role in lupus pathogenesis (9). Female lpr mice had a significantly lower abundance of *Lactobacillales* than MRL controls at 5 wk of age, prior to the onset of lupus-like disease, and MRL-to- lpr cecal transplantation led to a significantly reduced production of autoantibodies anti-double-stranded DNA (anti-dsDNA) (10). Moreover, treatment of female lpr mice with a mixture of 5 *Lactobacillus* spp. reduced disease activity, improved renal function, and prolonged survival of these mice. These protective effects were linked to changes in the immune response (10). In addition, antibiotic treatment initiated postdisease onset, ameliorated lupus-like symptoms that significantly altered the composition of gut microbiota, and, most notably, increased the relative abundance of *Lactobacillus* spp. (11). Recently, Mardani *et al.* (12) showed that the administration of the probiotics *Lactobacillus delbrueckii* or *Lactobacillus rhamnosus* to a pristane-induced SLE mouse model was able to prevent the initiation or the progression of the SLE disease. Nonetheless, neither the MRL/ lpr nor pristane-induced SLE mice became hypertensive (13, 14); therefore, their usefulness to examine mechanisms that lead to SLE hypertension and the effects of therapeutic treatments of hypertension in SLE were limited.

Female NZBWF1 mice have several characteristics consistent with human SLE, including immune complex deposition in the glomeruli, dsDNA autoantibodies, albuminuria, and, importantly, endothelial dysfunction and hypertension (13, 15, 16). Similarly to humans, the cause of SLE in this model is thought to be polygenic, and female NZBWF1 mice are more prominently affected than males (17). In these female mice, endothelial dysfunction occurs before high blood pressure (BP), which is not dependent on glomerulonephritis (15). Recent studies showed that the composition of gut microbiota changed markedly from before to after the onset of lupus disease in these SLE mice (8). Moreover, *Lactobacillus paracasei* GMNL-32, *L. reuteri* GMNL-89, and *L. reuteri* GMNL-263 significantly increased serum antioxidant activity in NZB/W F1 mice, reduced proinflammatory cytokine levels, and attenuated hepatic TLR (4, 5, 7, 9) and MyD88 signaling, which suggests that these specific *Lactobacillus* strains can be used as part of a comprehensive treatment of SLE patients (18). However, no information about the effects of these strains on BP has been found in NZB/W F1 mice.

We have recently demonstrated that the modification of microbiota through the administration of *Lactobacillus fermentum* CECT5716 (LC40). This bacterium was originally isolated from human milk (19), and its probiotic potential, survival in gastrointestinal conditions, adhesion to intestinal cells, and antimicrobial activity have also been described (20). Therefore, this strain is a good candidate for functional food and pharmaceutical products. In addition, this probiotic strain reduced BP in spontaneously hypertensive rats (21) and in hypertensive mice induced by tacrolimus (22), improving gut barrier function and T helper cell (T_H)₁₇/regulatory T cell (T_{reg}) balance in

mesenteric lymph nodes (23). Therefore, in the present study, we tested a hypothesis, posing that the treatment with the probiotic LC40 might ameliorate disease activity and cardiovascular complications through the modulation of the composition of intestinal microbiota and the immune system in female NZBWF1 mice.

MATERIALS AND METHODS

The investigation conforms to the National Institutes of Health (NIH; Bethesda, MD, USA) *Guide for the Care and Use of Laboratory Animals* and was approved by the Ethics Committee of Laboratory Animals of the University of Granada (Granada, Spain; Ref. 459-bis-CEEA-2012).

Preparation and administration of the probiotic

LC40, as a freeze-dried preparation containing 2×10^{11} colony forming units (CFUs)/g, was supplied by Biosearch Life (Granada, Spain). LC40 was suspended using a sterile PBS solution and was diluted to obtain a concentration of 5×10^9 CFUs in 1 ml for use in experimental protocols, as previously described (23).

Animals and experimental groups

Eighteen-week-old female NZBWF1 (SLE) and NZW/LacJ (control) mice from The Jackson Laboratory (Bar Harbor, ME, USA) were randomly assigned to 4 different groups: control, control-treated (control + LC40), SLE, and SLE-treated (SLE + LC40). Control-treated and SLE-treated mice received vehicle (PBS) or the probiotic LC40, respectively, at a dosage of 5×10^8 CFUs daily in 0.1 ml by using an oral gavage for 15 wk. Mice were maintained in a specific pathogen-free environment. Mice were provided with water and a standard laboratory diet (Safe DS A04; Safe, Augy, France) *ad libitum*.

BP measurements, physical characteristics, heart and kidney weight indices

Systolic BP (SBP) was measured in conscious mice by tail-cuff plethysmography using a digital pressure meter (LE 5001; Leika Geosystems, Barcelona, Spain). At least 7 replicates/mouse of the SBP were obtained in every session, and the mean of the lowest 3 values within 5 mmHg was considered the SBP level (24).

At the end of the experimental period, mice were subjected to isoflurane anesthesia. A polyethylene catheter containing 100 U heparin in sterile, isotonic NaCl solution was inserted into the left carotid artery. Intra-arterial BP was monitored in conscious mice under unrestrained conditions. Direct BP and heart rate (HR) were recorded continuously (MacLab; ADInstruments, Sydney, Australia). Twenty-four hours after inserting the catheter, intra-arterial BP was recorded continuously for 60 min with a sampling frequency of 400/s (MacLab; ADInstruments). Mean arterial BP and HR values recorded during the last 30 min were averaged for intergroup comparisons (25).

Body weight (in grams) was measured for all mice. The hearts were excised; the atria and the right ventricle were then removed, and the remaining left ventricle was weighted. The left ventricle, liver, spleen, gonadal and mesenteric fat, and kidney weight indices were calculated by dividing their weights by the tibia length. All tissue samples were snap-frozen in liquid nitrogen and then stored at -80°C .

Plasma parameters

At the end of the treatment, mice were euthanized under isoflurane anesthesia. Blood samples were collected from the heart, cooled on ice, and centrifuged for 10 min at 3500 rpm at 4°C. Then plasma samples were frozen at -80°C. Plasma glucose, triglycerides, HDL, and total cholesterol concentrations were measured by colorimetric methods using Spinreact kits (Spinreact, Girona, Spain). Plasma anti-dsDNA antibodies were measured following the manufacturer's instructions, as previously described (26). Plasma LPS concentration was measured using the Limulus Amebocyte Lyste Chromogenic Endotoxin Quantitation Kit (Lonza Group, Basel, Switzerland) according to the manufacturer's instructions. Plasma cytokines were measured by a multiplex assay using luminex technology (MilliporeSigma, Burlington, MA, USA).

Vascular reactivity studies

Descending thoracic aortic rings were resected from the animals and were suspended in a wire myograph (model 610M; Danish Myo Technology, Hinnerup, Denmark) for isometric tension measurement as previously described (22). The organ chamber was filled with Krebs solution (composition in mM: 118 NaCl, 4.75 KCl, 25 NaHCO₃, 1.2 MgSO₄, 2 CaCl₂, 1.2 KH₂PO₄, and 11 glucose) at 37°C and gassed with 95% O₂ and 5% CO₂ (pH ~7.4). Length-tension characteristics were obtained *via* the myograph software (Myodaq v.2.01), and the aortas were loaded to a tension of 5 mN.

In endothelium-intact aorta, cumulative concentration-response curves to acetylcholine (1 nM to 10 μM) were constructed in intact rings precontracted by the thromboxane A₂ analog U46619 (10 nM). A second concentration-relaxant response curve to acetylcholine was performed in each ring in the absence or in the presence of eNOS inhibitor N^G-nitro-L-arginine methyl ester (L-NAME, 100 μM), or the specific pan-NADPH oxidase [(NOX) inhibitor VAS2870 (5 μM)]. The relaxation responses to sodium nitroprusside (SNP, 1 nM to 10 μM) were studied in the dark in endothelium-denuded vessels precontracted with U46619 (10 nM). Relaxation responses to acetylcholine and SNP were expressed as percentages of precontraction induced by U46619. Aorta was denuded of endothelium by gently rubbing the intimal surface with a needle. The absence of functional endothelium was tested by observing no relaxation response to acetylcholine.

In situ detection of vascular reactive oxygen species production and NOX activity

Unfixed thoracic aortic rings were cryopreserved (0.1 M PBS plus 30% sucrose for 1–2 h), embedded in optimal cutting temperature compound (Tissue-Tek; Sakura Finetechnical, Tokyo, Japan), and frozen at -80°C. Then, 10-μm cross sections were obtained in a cryostat (Model HM 500 OM; Microm International, Walldorf, Germany). Sections were incubated for 30 min in 4-(2-hydroxyethyl)-1-piperazineethanesulfonic acid (HEPES) buffer solution containing dihydroethidium (DHE, 10 μM), counterstained with the nuclear stain DAPI (300 nM), and, in the following 24 h, examined under a fluorescence microscope (DM IRB; Leica Microsystems, Buffalo Grove, IL, USA). Sections were photographed, and ethidium and DAPI fluorescences were quantified using ImageJ (v.1.32j; NIH; <http://rsb.info.nih.gov/ij/>). Reactive oxygen species (ROS) production was estimated from the ratio of ethidium/DAPI fluorescence (24). In preliminary experiments, before incubation with DHE, serial sections were treated with either the O₂⁻ scavenger polyethylene glycol-modified

superoxide dismutase (25 U/ml) for 30 min at 37°C, indicating the specificity of this reaction.

The lucigenin-ECL assay was used to determine NOX activity in intact aortic rings as previously described (16). Aortic rings from all experimental groups were incubated for 30 min at 37°C in HEPES-containing physiologic saline solution (pH 7.4) of the following composition (in mM): NaCl 119, HEPES 20, KCl 4.6, MgSO₄ 1, Na₂HPO₄ 0.15, KH₂PO₄ 0.4, NaHCO₃ 1, CaCl₂ 1.2, and glucose 5.5. Aortic production of O₂⁻ was stimulated by the addition of NADPH (100 μM). Rings were then placed in tubes containing physiologic saline solution, with or without NADPH. Then lucigenin was injected automatically at a final concentration of 5 μM to avoid artifacts occurring at higher concentrations. NOX activity was determined by measuring luminescence over 200 s in a scintillation counter (Lumat LB 9507; Berthold Technologies, Bad Wildbad, Germany) in 5-s intervals and was calculated by subtracting the basal values from those found in the presence of NADPH. Vessels were then dried, and dry weight was determined. NOX activity is expressed as relative luminescence units per minute per milligram of dry aortic tissue.

RT-PCR analysis

For RT-PCR analysis, total RNA was extracted from aorta and colon by homogenization and converted into cDNA by standard methods. Tissues were homogenized in 1 ml of Tri Reagent (Thermo Fisher Scientific, Waltham, MA, USA). RNA isolation was performed with traditional methods using sequential washes with bromochloropropane, isopropanol, and ethanol 75%. RNA concentrations were measured with a NanoDrop 2000 Spectrophotometer (Thermo Fisher Scientific). PCR was performed with a Techgene thermal cycler (Techne, Cambridge, United Kingdom). A quantitative real-time RT-PCR technique was used to analyze mRNA expression. The sequences of the sense and antisense primers used for amplification are described in Supplemental Table S1. Preliminary experiments were carried out with various amounts of cDNA to determine nonsaturating conditions of PCR amplification for all the genes studied. Therefore, under these conditions, relative quantification of mRNA was assessed by the RT-PCR method used in this study. The efficiency of the PCR reaction was determined using a dilution series of a standard tissue sample. Quantification was performed using the ΔΔC_t method. The housekeeping gene glyceraldehyde-3-phosphate dehydrogenase and ribosomal protein L13 were used for internal normalization (24).

Western blotting analysis

We examined the state of eNOS and Ras homolog gene family, member A (RhoA) protein expression in aortic homogenates. Aortic homogenates were run on a sodium dodecyl sulfate-polyacrylamide electrophoresis (40 μg of protein/lane), then proteins were transferred to PVDF membranes, incubated with a primary rabbit monoclonal anti-p-eNOS-Ser¹¹⁷⁷ antibody (Cell Signaling Technology, Danvers, MA, USA), a rabbit monoclonal anti-p-eNOS-Thr⁴⁹⁵ (MilliporeSigma), or a mouse monoclonal anti-eNOS antibody (BD Biosciences, San Jose, CA, USA) and rabbit polyclonal anti-RhoA (Abcam, Cambridge, United Kingdom). All antibodies were used at 1/1000 dilution and incubated overnight at 4°C. Then membranes were incubated with secondary peroxidase-conjugated goat anti-rabbit or goat anti-mouse antibodies (1:2000; Santa Cruz Biotechnology, Santa Cruz, CA, USA). Antibody binding was detected by an ECL system (Amersham, Little Chalfont, United Kingdom), and the densitometric analysis was performed using Scion Image-Release Beta 4.02 software (<http://www.scioncorp.com>). Phosphorylated eNOS/eNOS and RhoA/α-actin abundance ratios were calculated,

and data were expressed as a percentage of the values in control aorta from the same gel (24).

Flow cytometry

Mesenteric lymph nodes and spleens were collected from mice. The tissues were properly mashed with wet slides to decrease friction. The solutions were then filtered through a cell strainer of 70 μm . Cells from spleens were isolated, and then the red blood cells were lysed with Gey's solution. For intracellular staining, 1×10^6 cells were counted and incubated with a protein transport inhibitor (BD GolgiPlug; BD Biosciences) for an optimum detection of intracellular cytokines by flow cytometry, and cells were stimulated with 50 ng/ml phorbol 12-myristate 13-acetate plus 1 μg /ml ionomycin. After 4.5 h, cell aliquots from each sample were blocked with Fc- γ receptors, blocking for 30 min at 4°C to avoid nonspecific binding to mouse Fc- γ receptors. After that, cells were transferred to polystyrene tubes for surface staining with anti-CD4 (PerCP-Cy, clone RM4-5; BD Biosciences), anti-CD45 (APE-eFluor 780, clone 30-F11; BD Biosciences), anti-B220 (allophycocyanin, clone RA3-6B2; BD Biosciences), and viability dye (allophycocyanin-Cy7, clone N418; Thermo Fisher Scientific) for 20 min at 4°C in the dark. The lymphocytes and splenocytes were then fixed, permeabilized, and intracellular staining was conducted with mAbs anti-FoxP3 (PE, clone FJK-16s; Thermo Fisher Scientific), anti-IL-17a (PE-Cy7, clone eBio17B7; Thermo Fisher Scientific), and anti-IFN- γ (Alexa Fluor 488, clone XMG1.2; Thermo Fisher Scientific) for 30 min at 4°C in the dark. Data collection was performed using a flow cytometer Canto II (BD Biosciences) as previously described (16, 22). Supplemental Figure S1 illustrates the gating strategy that was applied.

L. fermentum CECT5716 detection

Fecal samples were suspended at 200 mg/ml in buffered peptonized water (BioMérieux, Marcy-l'Étoile, France) and used to inoculate De Man, Rogosa and Sharpe broth (Scharlab, Barcelona, Spain). In order to enrich *Lactobacillus* spp populations, De Man, Rogosa and Sharpe broth pH was adjusted at 4.5 with acetic acid. Cultures of 15 ml of broth medium containing fecal samples (0.25 ml) or buffered peptonized water (0.25 ml; negative controls) were incubated for 48 h at 37°C under anoxic conditions (27). Microbial biomass from those cultures with positive growth was collected by centrifugation (4500 g for 10 min) and used as raw material for bacterial DNA purification using the Ezna Stool DNA Purification Kit (Omega Bio-Tek, Norcross, GA, USA). Bacterial DNA samples were used as templates in SYBR green-based quantitative PCR assays in 20- μl reactions containing 10- μl master mix (FastStart Essential DNA Green Master; Roche, Basel, Switzerland); 1 μl bacterial DNA as template and the oligonucleotides (Eurofins Genomics, Louisville, KY, USA) L677 and L159 (*Lactobacillus* spp.) (28) or HSL40_126F and HSL40_126R (LC40) (29) as primers (500 nM). Amplification and detection were performed in a Stratagene MX3005P thermal cycler (Fisher Scientific, Madrid, Spain). Positive samples (presence of *Lactobacillus* spp., LC40, or both) showed amplification reactions with C_t values below 35 cycles and amplicons with the expected melting temperature.

DNA extraction, 16S rRNA gene amplification, bioinformatics

Fecal samples were collected from 4 to 8 animals/group at the end of the experimental period. DNA was extracted from fecal samples using G-spin columns (Intron Biotechnology, Gyeonggi-do, Korea) starting from 30 mg of samples resuspended in PBS

and treated with proteinase K and RNases (30). DNA concentration was determined in the samples using Quant-IT PicoGreen reagent (Thermo Fisher Scientific), and DNA samples (about 3 ng) were used to amplify the V3–V4 region of 16S rRNA gene (31). PCR products (~450 base pair included extension tails, which allowed sample barcoding and the addition of specific Illumina sequences in a second low-cycle number PCR. Individual amplicon libraries were analyzed using a Bioanalyzer 2100 (Agilent Technologies, Santa Clara, CA, USA), and a pool of samples was made in equimolar amounts. The pool was further cleaned and quantified, and the exact concentration estimated by real-time PCR (Roche). Finally, DNA samples were sequenced on an MiSeq instrument (Illumina, San Diego, CA, USA) with 2×300 paired-end read sequencing at the Unidad de Genómica (Parque Científico de Madrid, Madrid, Spain).

We used the barcoded Illumina paired-end sequencing pipeline to process the raw sequences (32). First, the barcode primers were trimmed and filtered if they contained ambiguous bases or mismatches in the primer regions according to the barcoded Illumina paired-end sequencing protocol. Second, we removed any sequences with more than 1 mismatch within the 40–70 base pair region at each end. Third, we used 30 Ns to concentrate the 2 single-ended sequences for the downstream sequence analysis. A detailed description of these methods was reported previously (33). Fourth, we performed UCHIME (implemented in USEARCH, v.6.1) to screen out and remove chimeras in the *de novo* mode (using-minchunk 20-xn 7-noskip-gaps 2) (34).

Between 90,000 and 220,000 sequences were identified in each sample. All subsequent analyses were performed using 16S Metagenomics (v.1.0.1.0) from Illumina. The sequences were then clustered to an operational taxonomic unit (OTU) using USEARCH with default parameters (USERACH v.61). The threshold distance was set to 0.03. Thus, when the similarity between 2 16S rRNA sequences was 97%, the sequences were classified as the same OTU. Quantitative Insights Into Microbial Ecology (QIIME)-based alignments of representative sequences were performed using PyNASt, and the Greengenes 13.8 database was used as the template file. The Ribosome Database project algorithm was applied to classify the representative sequences into specific taxa using the default database (34). The Taxonomy Database (National Center for Biotechnology Information) was used for classification and nomenclature. Bacteria were classified based on the short-chain fatty acids' end-product, as previously described (35, 36).

Statistical analysis

The Shannon diversity, Chao richness, and Pielou evenness, and observed species indexes were calculated using the QIIME pipeline (PAST $\times 3$). Reads in each OTU were normalized to total reads in each sample. Only taxa with a percentage of reads $>0.001\%$ were used for the analysis. Partial Least Square (PLS) analysis was also applied to these data to identify significant differences between groups. Linear discriminant analysis (LDA) scores above 2 were displayed. Taxonomy was summarized at the genus level within QIIME v.1.9.0 and uploaded to the Galaxy platform (37) to generate LEfSe/cladogram enrichment plots that considered significant enrichment at a value of $P < 0.05$, LDA score >2 .

Results are expressed as means \pm SEM. Statistical analyses were performed using Prism 7 (GraphPad software, La Jolla, CA, USA). A 2-way ANOVA (with Sidak's correction for comparison of multiple means) was used for comparisons of 4 groups with 2 variables (SLE and LC40 treatments). A 2-way ANOVA with repeated measurements approach (with Tukey's correction for comparison of multiple means) was used for comparisons of vasodilator potency. Significance was accepted at $P < 0.05$.

RESULTS

LC40 treatment prevents gut dysbiosis in SLE mice

LC40 was detected alive in fecal samples of 57% and 50% of SLE-LC40 and control-LC40 groups, respectively, demonstrating that this strain is able to survive the conditions of the gastrointestinal tract of these mice. We analyzed fecal DNA isolated from all experimental mice groups to determine the dynamics of gut microbiota during lupus disease. In order to compare the bacterial composition of the gut microbiota between SLE mice and control mice, we have evaluated 3 major ecological parameters, including Shannon and Simpson (the combined parameters of richness and evenness) diversity, Chao richness (an estimate of a total number of OTUs present in the given community), Pielou evenness (to show how evenly the individuals in the community are distributed over different OTUs), and number of species. No

significant changes among groups were observed regarding microbial richness, diversity, and evenness (Fig. 1A).

Similarly, when we evaluated the phyla composition, fecal samples were dominated by Firmicutes and Bacteroidetes, and smaller proportions of Actinobacteria, Proteobacteria, and Tenericutes (Fig. 1B) were found in the different experimental groups. No significant differences were found between control and SLE group in the 2 main phyla percentages (Fig. 1B and Supplemental Table S2) and F/B ratio (Fig. 1C). Of note, the administration of the probiotic LC40 to the SLE-treated group was able to reduce the F/B ratio (Fig. 1C) as a result of a decrease in the proportion of Firmicutes and an increase in the proportion of Bacteroidetes. We have also evaluated what genera of bacteria contributed to the alteration of microbiota composition in SLE disease. A significant decrease in the proportion of butyrate- and acetate-producing bacteria has been previously described in both humans and animals with hypertension (38). However, we did not find any differences in the proportion of butyrate-, acetate-, and

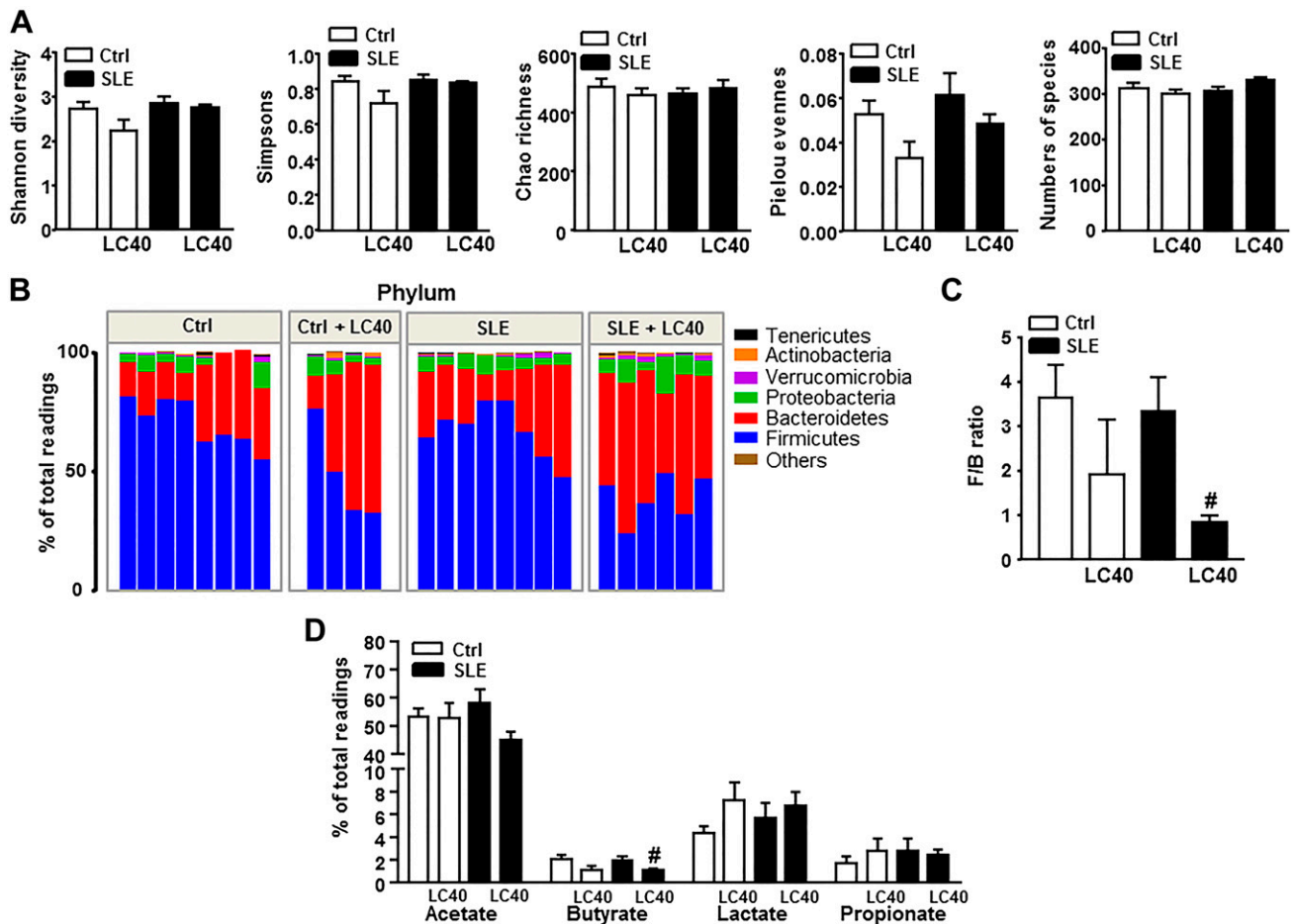


Figure 1. Effects of LC40 treatment on phyla changes in the microecological parameters and gut microbiota composition. Fecal samples were collected and bacterial 16S ribosomal DNA were amplified and sequenced to analyze the composition of microbial communities. A) Fecal diversity, richness, evenness, and numbers of species were used to evaluate general differences of microbial composition in all experimental groups. B) Phylum breakdown of the most abundant bacterial communities in the fecal samples from all experimental groups. C) The F/B ratio was calculated as a biomarker of gut dysbiosis. D) Relative proportions of lactate-, butyrate-, and acetate-producing bacteria in the gut microbiota in control (Ctrl) and SLE mice. Values are expressed as means \pm SEM ($n = 4-8$). * $P < 0.05$ compared with the Ctrl group; [#] $P < 0.05$, ^{##} $P < 0.01$ compared with the untreated SLE group.

lactate-producing bacteria between SLE mice and control mice. Only the LC40 treatment reduced the proportion of butyrate-producing bacteria in SLE mice (Fig. 1D). Supplemental Figure S2 shows the bacterial taxa (class, order, family, and genus) that were altered by SLE disease, according to LEfSe analysis. Prominent changes in bacterial taxa occurred, as showed in cladograms comparing control with SLE groups (Supplemental Fig. S2A) and SLE with SLE-LC40 groups (Supplemental Fig. S2B), with minor changes between SLE and control mice (4 increased and 2 decreased) and SLE treated with LC40 vs. SLE (4 increased and 1 decreased) when we compared by LDA score genera representing >0.1% of total bacteria.

We have also evaluated what genera of bacteria were altered within the microbiota (Fig. 2). Figure 2A shows 3-

dimensional scatterplots generated by principal coordinate analysis to visualize whether the experimental groups in the input phylogenetic tree have significantly different microbial communities between each other. The main separation is due to LC40 treatment, wherein control and SLE groups did not separate in genera. Interestingly, and similar to that described in LDA analysis, we found that the gut microbiota of SLE mice had a significantly higher abundance of only *Pedobacter*, *Lactobacillus*, and *Prevotella* than the control group, and no changes in other genera, such as *Bifidobacterium*, were found (Fig. 2B, C). LC40 treatment increased the accumulation of *Parabacteroides* or *Bifidobacterium* (Fig. 2C) in both control-treated and SLE-treated mice. This modification would be involved in the change in T-cell polarization (39)

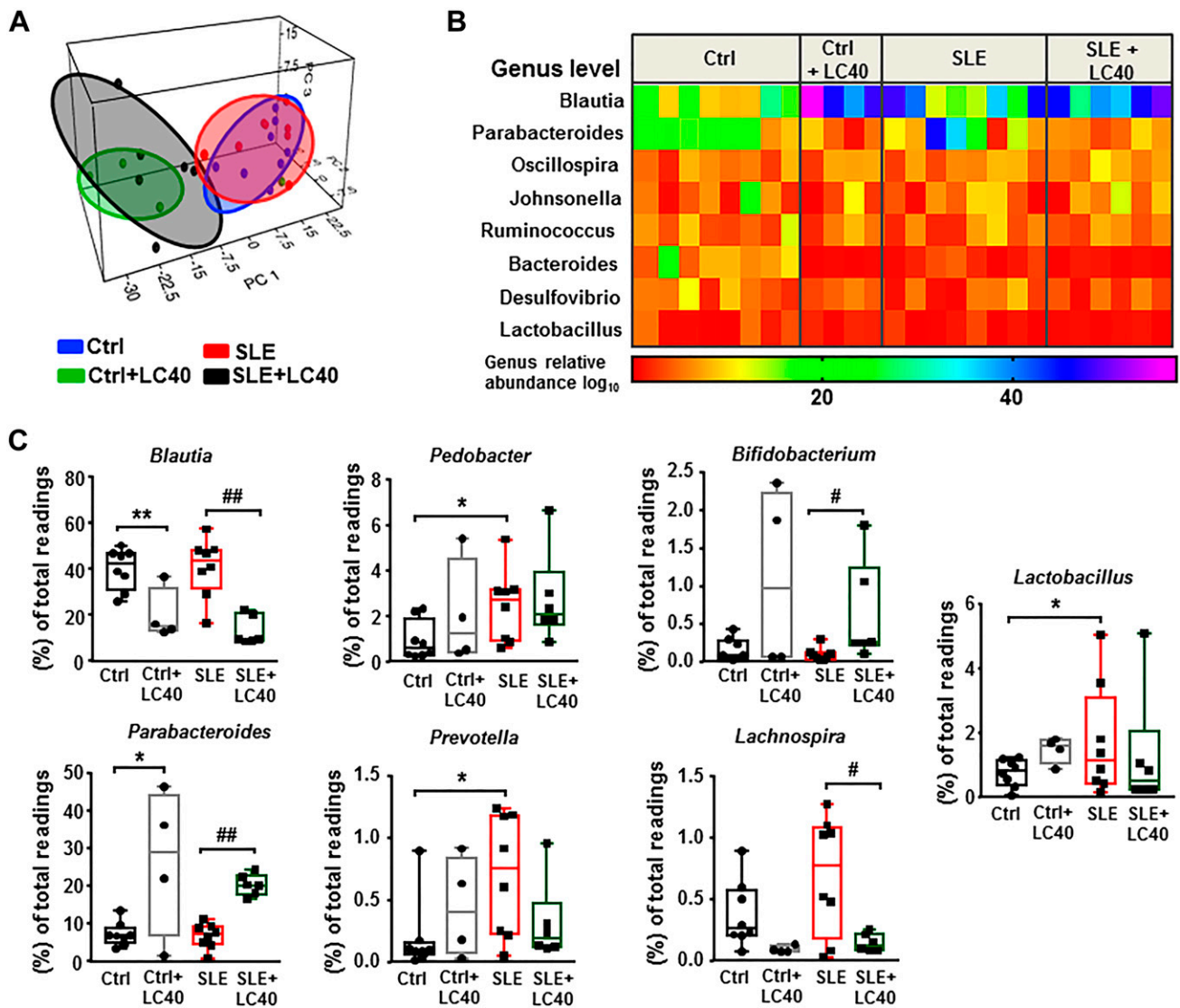


Figure 2. Effects of LC40 treatment on genera changes in the gut microbiota composition. *A*) Principal coordinate analysis in the gut microbiota from all experimental groups. *B*) Heatmap showing the bacterial genera most differing in abundance between different groups. Samples clustered by treatment group demonstrated that the treatments resulted in distinct populations of bacteria at the genus level. The heatmap colors represent the relative percentage of microbial genus assigned within each sample. *C*) Bacterial genera *Blautia*, *Pedobacter*, *Bifidobacterium*, *Lactobacillus*, *Parabacteroides*, *Prevotella*, and *Lachnospira* in the gut microbiota in control (Ctrl) and SLE mice. Values are expressed as means ± SEM (n = 4–8). *P < 0.05, **P < 0.01 compared with the Ctrl group; #P < 0.05, ##P < 0.01 compared with the untreated SLE group.

found in mesenteric lymph nodes induced by this probiotic and the improvement of gut epithelial integrity by strengthening tight junctions (40). Moreover, we observed that the administration of LC40 significantly reduced the abundance of *Blautia* and *Lachnospira* (Fig. 2C) in the gut microbiota of SLE-treated mice.

LC40 treatment improves intestinal integrity, inflammation, and endotoxemia

We measured endotoxin levels in plasma and found them significantly higher in SLE mice than in the control group (Fig. 3A). Interestingly, the long-term treatment with LC40 significantly decreased endotoxemia in lupus mice. These results suggest that intestinal permeability is increased in this female mouse model of lupus and allows bacterial components (*e.g.*, LPS) to enter the blood stream. Because of this, we tested the integrity of the gut barrier and found that the treatment with LC40 significantly increased the colonic mRNA expression of barrier-forming junction transcripts (zonula occludens-1 and occludin) and of the mucins, in particular, mucin-2 (Fig. 3B). This effect suggests an enhanced barrier function of the intestinal epithelium as a result of the supplementation with *Lactobacillus*. We also found that colonic expression of IL-18 (Fig. 3C), a cytokine important for tissue repair (41) and limiting colonic T_H17 cell differentiation (42), was higher in SLE-treated mice. Furthermore, the increased mRNA levels of the colonic proinflammatory cytokines TNF- α and IL-1 β (Fig. 3D) in SLE mice were significantly reduced by LC40 administration. In addition, the colonic expression of intestinal alkaline phosphatase (IAP) was significantly up-regulated after the probiotic treatment

in SLE mice compared with untreated lupus mice (Fig. 3E). This effect may be associated with the enhanced LPS clearance because IAP is an enzyme expressed on the microvillus membranes of enterocytes (43) that can dephosphorylate LPS, leading to an important reduction in LPS toxicity (44).

LC40 treatment improves morphologic variables, plasma parameters, and BP

At 18-wk old, SBP was similar among all experimental groups (unpublished data). At 33 wk, SBP was significantly higher in SLE mice compared with control mice in ~56 mmHg, and this change was prevented by chronic LC40 treatment (Fig. 4A). Also, these antihypertensive effects were observed using direct intra-arterial recordings in conscious mice (Fig. 4B), without significantly affecting HR (Fig. 4C). Regardless of the presence or absence of LC40 treatment, a significant increase in body weight of SLE mice in comparison with the weight of control animals was found (Supplemental Table S3). Anatomic analysis revealed that left ventricle weight/tibia length, heart weight/tibia length and kidney weight/tibia length indices were higher in SLE mice (Supplemental Table S3) than in control mice. Long-term administration of LC40 significantly reduced both renal and cardiac hypertrophy found in SLE mice. Analysis of metabolic plasma variables (Supplemental Table S3) showed that fasting glycemia and plasma cholesterol were higher in SLE mice than in control mice. However, no effect of LC40 treatment was found on basal glycemia and cholesterol.

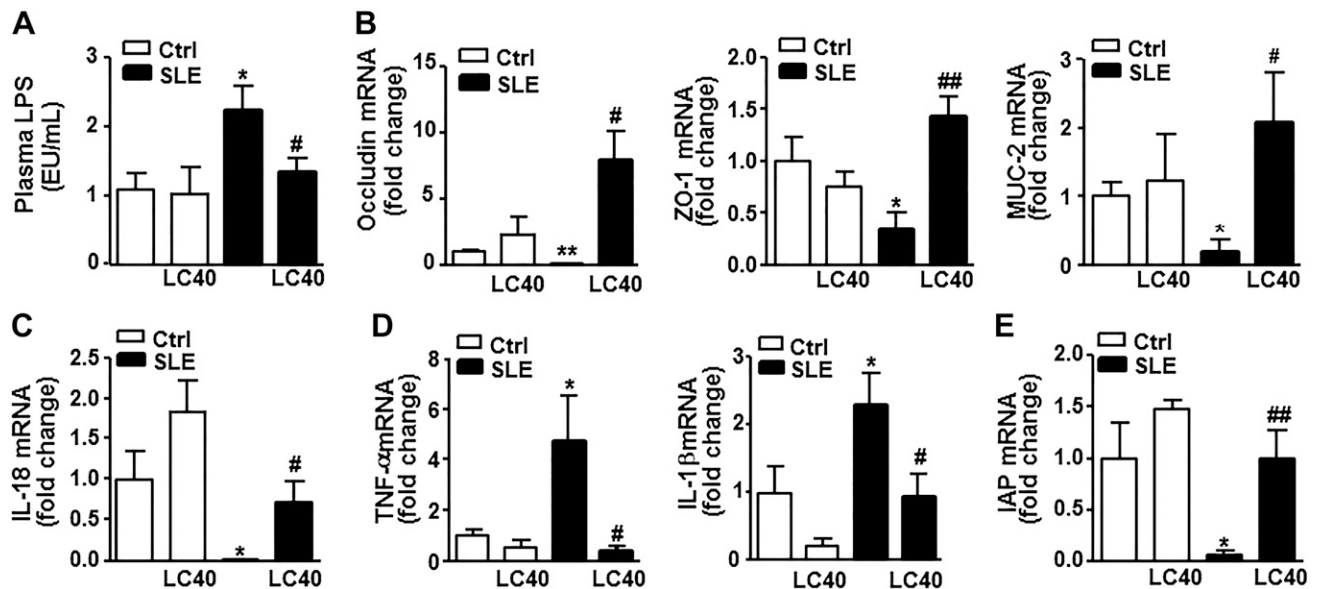


Figure 3. Effects of LC40 treatment on proinflammatory and epithelial integrity markers. A) Plasma endotoxin concentrations (EU/ml, endotoxin U/ml). B–D) Colonic mRNA levels of occludin, zonula occludens-1 (ZO-1), and mucin (MUC)-2 (B), tissue repair cytokine IL-18 (C), proinflammatory cytokines TNF- α and IL-1 β (D). E) IAP in control (Ctrl) and SLE mice. Values are expressed as means \pm SEM ($n = 4-6$). * $P < 0.05$, ** $P < 0.01$ compared with the Ctrl group; # $P < 0.05$, ## $P < 0.01$ compared with the untreated SLE group.

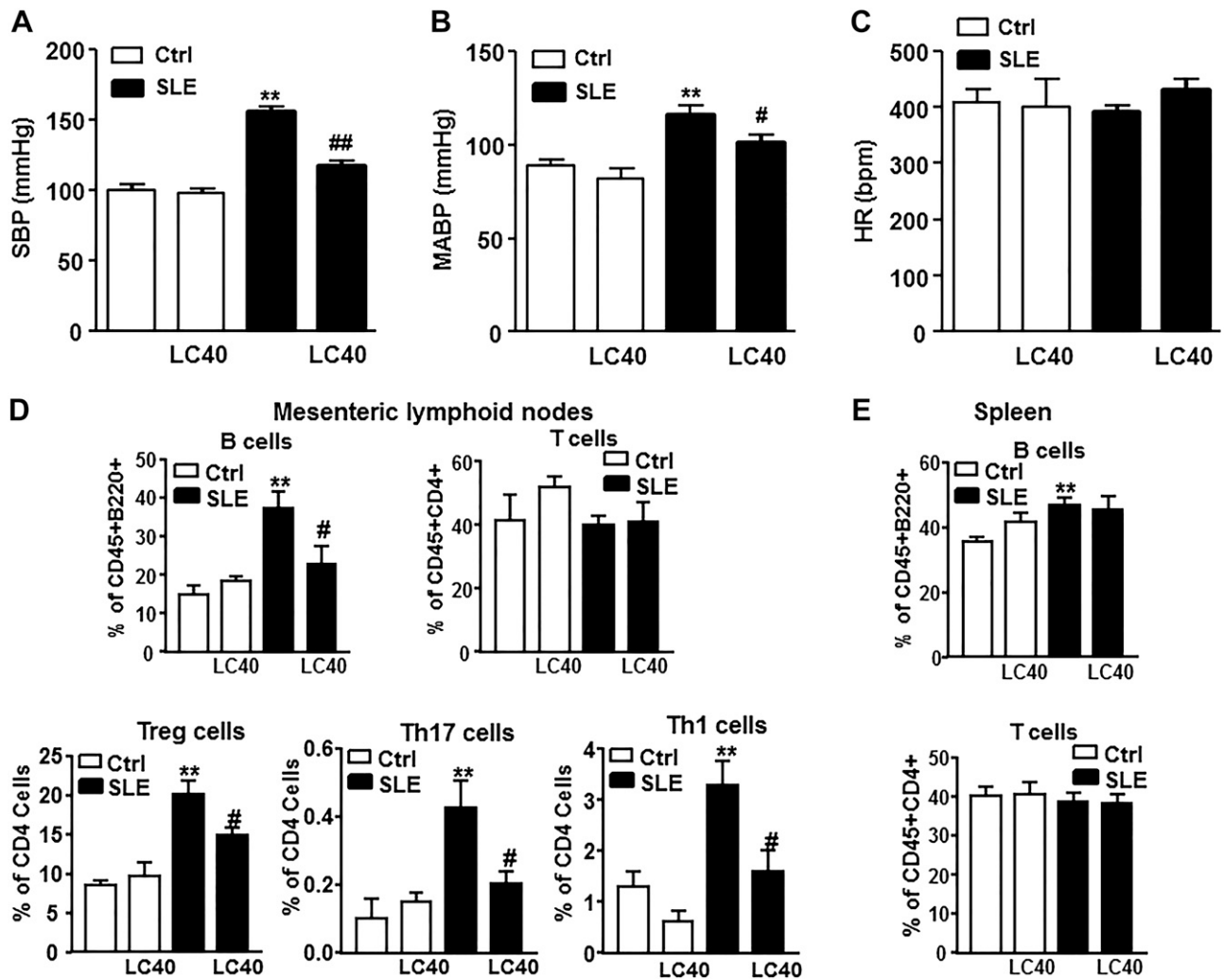


Figure 4. Effects of LC40 treatment on both BP and lymphocytes populations in mesenteric lymph nodes and spleen. *A*) SBP was measured by tail-cuff plethysmography. *B*, *C*) Mean arterial BP (MABP) (*B*) and HR (*C*) were measured in left carotid artery by direct registration in control (Ctrl) and SLE mice. *D*, *E*) Total B (B220⁺) lymphocytes, T cells (CD4⁺), T_{reg} cells (CD4⁺ FoxP3⁺), T_h17 (CD4⁺ IL-17a⁺), and T_h1 (CD4⁺ IFN- γ ⁺) cells measured by flow cytometry in mesenteric lymphoid nodes (*D*), and B and T cells in spleen (*E*) in Ctrl and SLE mice. Values are expressed as means \pm SEM ($n = 4-8$). ** $P < 0.01$ compared with the Ctrl group; # $P < 0.05$, ## $P < 0.01$ compared with the untreated SLE group.

LC40 treatment attenuates SLE disease activity and T cells imbalance

We measured SLE disease activity by plasma levels of autoantibodies, and we found a significant increase in SLE mice compared with control mice (Supplemental Fig. S3A), as previously reported (25). Probiotic treatment significantly reduced the levels of anti-dsDNA in SLE, being without effect in control mice. Moreover, disease progression has been associated with splenomegaly, most probably because of a lymphoproliferative disorder (45). We have also observed splenomegaly in lupus mice, which was considerably reduced by the administration of LC40 (Supplemental Fig. S3B).

Increased production of autoantibodies and progressive lupus-like autoimmune disease are associated with an imbalance of T cells (46) and increased B cells (47). In order to determine the immunomodulatory actions of the probiotic LC40, we measured the levels of B and T cells in

mesenteric lymph nodes and spleen from all experimental groups. The percentage of B cells was higher in both organs from SLE mice than in the control group, without any change in T cells (Fig. 4*D*, *E*). LC40 treatment of SLE mice led to a significant decrease in the levels of B cells in mesenteric lymph nodes (Fig. 4*D*), whereas this decrease was not found in the spleen (Fig. 4*E*). As expected, the percentages of T_{reg} (CD4⁺/FoxP3⁺) cells, T_h17 cells (CD4⁺/IL-17a⁺), and T_h1 (CD4⁺/IFN- γ ⁺) cells increased in SLE mice in mesenteric lymph nodes (Fig. 4*D*), whereas only T_{reg} cells increased by lupus disease in the spleen (Supplemental Fig. S4). LC40 treatment prevented the altered T-cell polarization induced by SLE only in mesenteric lymph nodes (Fig. 4*D*).

Plasma levels of IL-17a, IL-10, IFN- γ , TNF- α , and IL-21 also increased in SLE mice compared with control mice. Again, probiotic administration led to the return to normal levels of these parameters, except for TNF- α , which

tended to decrease but without statistical significance (Supplemental Fig. S5). The lower colonic TNF- α levels found in the SLE-LC40 group might be a result of a local anti-inflammatory activity induced by LC40 in the gut.

LC40 treatment prevents endothelial dysfunction and vascular oxidative stress

Aortas from SLE mice had strongly reduced endothelium-dependent vasodilator responses to acetylcholine compared with aortas from the control group. The treatment of SLE mice with the probiotic showed an increase in the acetylcholine-induced vasodilation compared with vehicle-treated SLE mice (Fig. 5A). The relaxation response induced by acetylcholine was fully inhibited by L-NAME in all experimental groups (Supplemental Fig. S6A), which shows that acetylcholine-induced relaxation of aorta depends entirely on endothelium-derived NO in both control and SLE groups. We determined the effects of SNP to analyze whether the impaired response to endothelium-derived NO is due to a

lower bioavailability of NO or to a defect in NO signaling in vascular smooth muscle. SNP directly activates soluble guanylate cyclase in vascular smooth muscle, mimicking the effects of endogenous NO. No differences were observed among all experimental groups in the endothelium-independent relaxation response to SNP (Supplemental Fig. S6B).

Ethidium red fluorescence was measured in sections of aortas incubated with DHE to characterize and localize ROS levels within the vascular wall. Positive red nuclei were observed in adventitial, medial, and endothelial cells from sections of aorta incubated with DHE (Fig. 5B). Nuclear ethidium red fluorescence was quantified and normalized to the blue fluorescence of the DAPI nuclear stain, allowing comparisons between different sections. Aortic rings from the SLE group showed a marked staining in adventitial, medial, and endothelial cells, whereas a slighter staining was found in aortic rings from the control group because it was almost suppressed in this group by the O₂⁻ scavenger polyethylene glycol-modified superoxide dismutase.

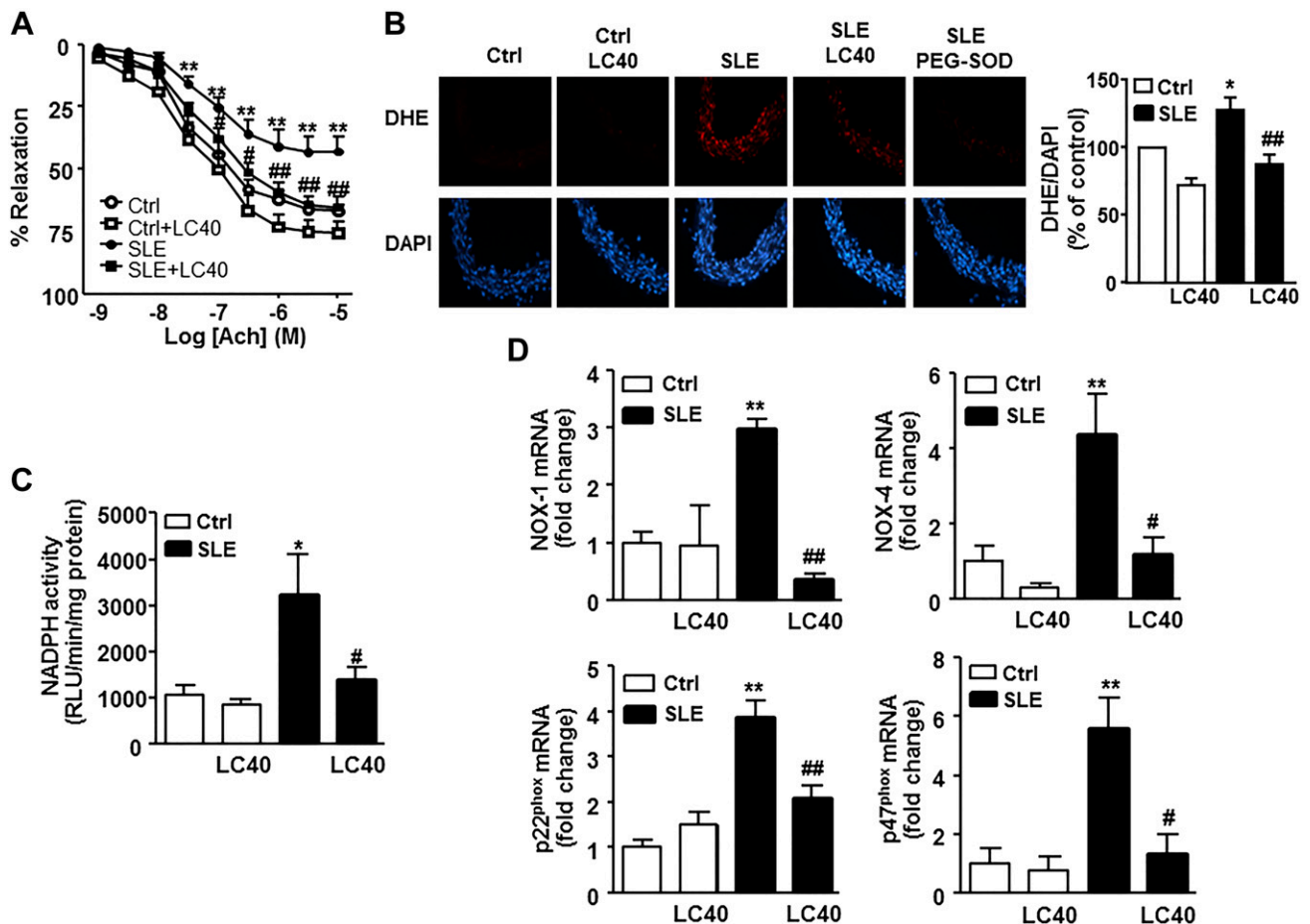


Figure 5. Effects of LC40 treatment on endothelial function, vascular oxidative stress, and NOX pathway. **A)** Vascular relaxation responses induced by acetylcholine (Ach) in endothelium-intact aortas precontracted by U46619 (10 nM) in control (Ctrl) and SLE mice. **B)** Top pictures show arteries incubated in the presence of DHE, which produces a red fluorescence when oxidized to ethidium by ROS. Bottom pictures show the blue fluorescence of the nuclear dye DAPI (original magnification, $\times 400$). Averaged values, mean \pm SEM ($n = 4-8$ rings from different mice) of the red ethidium fluorescence normalized to the blue DAPI fluorescence. **C, D)** NOX activity measured by lucigenin-ECL (**C**) and expression of NOX subunits NOX-1, NOX-4, p47^{phox}, and p22^{phox} (**D**) at the level of mRNA by RT-PCR in Ctrl and SLE mice. Values are expressed as means \pm SEM ($n = 4-8$). * $P < 0.05$, ** $P < 0.01$ compared with the Ctrl group; # $P < 0.05$, ## $P < 0.01$ compared with the untreated SLE group.

These effects on ROS levels were prevented by LC40 treatment (Fig. 5B). Because NOX is the major source of ROS in the vascular wall, we investigated the role of NOX-driven ROS production in endothelial function. We tested endothelium-dependent relaxation to acetylcholine in the presence of the pan-NOX inhibitor VAS2870. No significant differences in control and LC40-treated groups were observed after incubation with VAS2870, but this agent increased the relaxant response to acetylcholine in the SLE group, showing the critical role of increased NOX in the endothelial dysfunction found in aortas from SLE mice (Supplemental Fig. S6C). In addition, NOX activity was higher in the aortic rings of SLE mice than in the aortic rings of control mice (Fig. 5C). This activity was associated with a significant mRNA increase of the main NOX subunits in aortas obtained from all experimental groups (Fig. 5D). Chronic administration of LC40 reduced significantly both the up-regulation of NOX subunits and the increased NOX activity in SLE mice but not in control mice (Fig. 5C, D).

LC40 treatment reduces IL-17/Rho kinase/eNOS pathway and vascular inflammation

We measured the mRNA level of FoxP3 (a marker of T_{reg}) and ROR γ (a marker of T_{h17}) to determine whether these vascular effects were associated with T-lymphocyte infiltration in aortas. In addition, mRNA of IL-10 and IL-17a, cytokines released by T_{reg} and T_{h17} , respectively, were also measured. mRNA levels of FoxP3 and IL-10 were higher in SLE mice than in control mice. These mRNA levels were restored to normal values when SLE mice were treated with LC40 (Fig. 6A). Moreover, ROR γ and IL-17a mRNA levels were markedly higher in SLE mice than in control mice, whereas the chronic administration of LC40 decreased these high mRNA levels (Fig. 6B). IL-17a activates Rho A/Rho-kinase, leading to increased phosphorylation of the inhibitory eNOS residue Thr⁴⁹⁵ and endothelial dysfunction (48). Consistent with these data, we found that the protein expression of RhoA (Fig. 6C) (an upstream Rho-kinase activator) and eNOS phosphorylation at the inhibitory Thr⁴⁹⁵ were higher in SLE mice than

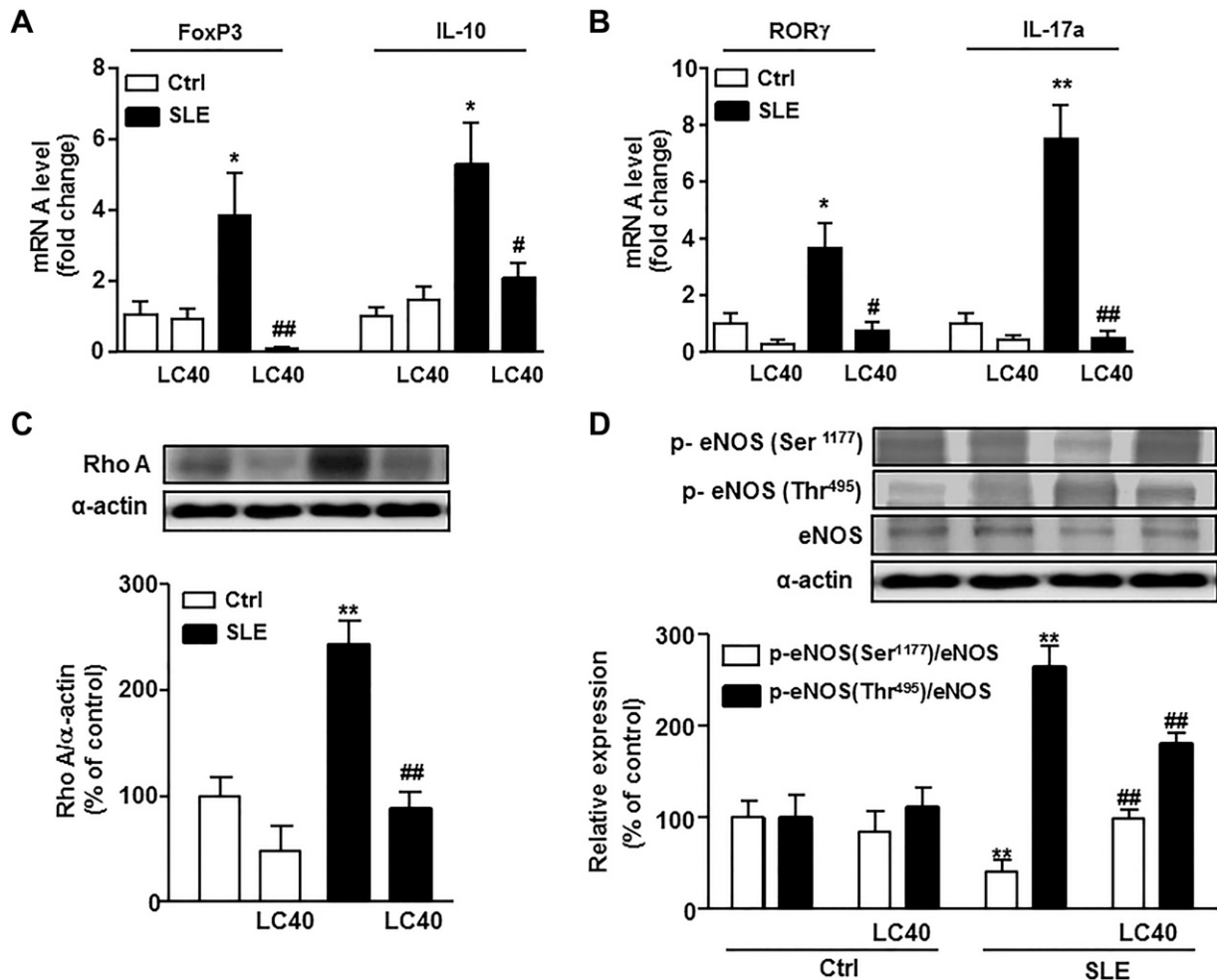


Figure 6. Effects of LC40 treatment on aortic T-cells infiltration. A) T_{reg} infiltration in aorta measured by FoxP3 and IL-10 mRNA levels. B) Aortic T_{h17} infiltration measured by mRNA levels of ROR γ and IL-17a. C) Rho-kinase activity measured by Rho protein expression. D) eNOS activity measured by Ser¹¹⁷⁷ and Thr⁴⁹⁵ eNOS phosphorylation in control (Ctrl) and SLE mice. Values are expressed as means \pm SEM ($n = 4-6$). * $P < 0.05$, ** $P < 0.01$ compared with the Ctrl group; # $P < 0.05$, ## $P < 0.01$ compared with the untreated SLE group.

in control mice, whereas the phosphorylation of eNOS at the activation site Ser¹¹⁷⁷ was lower in aortas of the SLE group than in aortas of the control group. These effects on SLE mice were restored to values similar to control mice when SLE mice were treated with LC40 (Fig. 6D).

Bacterial endotoxin LPS activates TLR-4, inducing cytokine expression in the vascular wall (49) and augmenting ROS production, primarily superoxide, which rapidly reacts with and inactivates NO in the vascular wall (24, 50). The mRNA levels of TLR-4 in aorta were significantly higher in SLE mice than in control mice. This increase was abolished by the LC40 treatment (Supplemental Fig. S7A). Furthermore, gene expression of the proinflammatory cytokines IL-6, IL-1 β , and TNF- α in aorta was higher in SLE mice than in control mice. Probiotic administration significantly reduced mRNA levels of these genes (Supplemental Fig. S7B).

DISCUSSION

We have demonstrated for the first time that chronic oral administration of the probiotic LC40 can improve the cardiovascular complications occurring in an experimental model of SLE with hypertension. The protective effects of LC40 are as follows: 1) a markedly attenuated lupus disease progression as evidenced by a decrease in splenomegaly, B cells accumulation, and plasma anti-dsDNA; 2) a significant decrease in SBP and heart and kidney hypertrophy; 3) a restoration of endothelial function associated with lower vascular T_h17 infiltration; and 4) an improvement of gut dysbiosis linked to increased colonic integrity and reduced endotoxemia. Herein, we suggest the important role of gut microbiota manipulation in preventing cardiovascular alterations associated with SLE.

Our results in gut microbiota composition are consistent with the relative higher abundance of a group of Lactobacilli found in the gut microbiota of NZBWF1 mice associated with deteriorated disease (8). However, these authors did not compare the fecal microbiota between NZBWF1 mice and a control mouse strain. In our experimental conditions, LC40 treatment significantly increased *Bifidobacterium* and *Parabacteroides* and significantly reduced *Lachnospira* and *Blautia*. Importantly, treatments improving lupus symptoms in lupus MRL/lpr mice restored gut colonization of *Lactobacillus spp.* and decreased that of *Lachnospiraceae* (10, 11).

In *lpr* mice, a leaky gut has been described (10), characterized by decreased expression of tight junction proteins, increased permeability, and increased plasma LPS levels. LPS accelerates lupus progression in several lupus-prone mouse models, including NZBWF1 mice, enhancing polyclonal B-cell activation, plasma anti-dsDNA antibodies, and renal failure (51, 52). A leaky gut may allow the translocation of Gram-negative bacteria across the intestinal epithelium, leading to an increase in LPS, a cell wall component of Gram-negative bacteria, into the circulation. Our data showed that the intestinal epithelium is compromised in lupus mice and that LC40 treatment can restore mucosal barrier

integrity. In addition, the effect of LC40 on gut barrier function may also be attributed to the increase of mucin-2, a mucin protein that functions primarily to protect the intestinal epithelium (53). Interestingly, LC40 treatment decreased LPS plasma levels. Consistently with previous data obtained from *lpr* mice treated with *Lactobacillus* (10), we have shown that the administration of *L. fermentum* to SLE mice was associated with a significant increase in the colonic expression of IAP, which has been reported to support the growth of Gram-positive bacteria (54), and might explain the increase of *Bifidobacterium* in SLE-treated mice. *Bifidobacterium* can also promote gut epithelial integrity by strengthening tight junctions (38). In conjunction, these results suggest that LC40 can restore intestinal mucosal barrier function, which is compromised in lupus mice.

Furthermore, humoral immune system activation plays a central role in the pathogenesis of SLE as pointed out by evidence suggesting that the number of B cells, which differentiate into antibody-producing plasma cells, is increased during SLE (47). IL-21 drives B-cell maturation and autoantibody production in rodent models of lupus (55). Accordingly, we found a higher number of B cells in both secondary lymphoid organs and a higher plasma level of IL-21 in SLE mice than in the control group. These changes were counteracted after LC40 treatment in SLE mice, that is, this probiotic treatment of SLE mice attenuated the size of the B-cell population in mesenteric lymph nodes. Furthermore, IL-18 inhibits B-cell antibody production (56), and abnormal activation of B cells might be related to IL-18 down-regulation found in the colons of SLE mice. Therefore, the increased IL-18 expression found in colonic samples of the SLE-LC40 group compared with the values found in SLE mice might also account to reduce B-cell activity in mesenteric lymph nodes, leading to lower plasma anti-dsDNA levels in the SLE-LC40 group than in the SLE group. Moreover, despite the elevated proportion of T_{reg} cells in aged lupus mice, these cells are ultimately unable to control the cumulative impact of multiple genetic elements driving lymphocyte activation and autoreactivity (57). The reduction induced by LC40 in T_{reg} cell counts might also decrease these processes, leading to a decrease of autoantibodies. The administration of a mouse anti-CD20 antibody (the equivalent of rituximab in humans) to deplete B cells markedly attenuates autoantibody production and prevents the development of hypertension in female NZBWF1 mice (58). Overall, reduced anti-dsDNA levels, mediated by B-cell depletion and lower activation might be involved in the antihypertensive effects of LC40 consumption. Moreover, an imbalance between anti-inflammatory T_{reg} and proinflammatory T_h17 cells is widely recognized as a cause in the establishment of both human SLE and murine lupus (59). A lower T_h17 count induced by LC40 might be related to an increase in IL-18 production from colonic tissue, an important cytokine for limiting colonic T_h17 cell differentiation in mesenteric lymph nodes (42).

Hypertension is often associated with impaired endothelial function, but whether this is causative in the progression of hypertension is difficult to prove. Recently, we have shown an impaired aortic endothelium-dependent

relaxation response to acetylcholine in NZBWF1 mice (16, 25) and a reduction in NO production induced by plasma from SLE patients with active nephritis in human endothelial cells (60). In consistency with this information, our data showed that chronic probiotic administration prevented the altered responses to acetylcholine observed in aortas from SLE mice and improved the reduced eNOS phosphorylation at the activation site Ser¹¹⁷⁷. Interestingly, the improvement in acetylcholine relaxation induced by LC40 in SLE mice was suppressed by L-NAME, indicating a protective role in NO bioactivity.

A crucial mechanism of endothelial dysfunction involves the vascular production of ROS, particularly O₂⁻, which reacts rapidly with NO and inactivates it (61). Herein, we found that ROS levels are increased in aortas from SLE mice and that LC40 decreased ROS content. The activity of NOX, which is considered the major source of O₂⁻ in the vascular wall, was markedly increased in SLE mice. NOX-driven ROS production is a key event in endothelial dysfunction in SLE because incubation with the selective NOX inhibitor VAS2870 increased the aortic endothelium-dependent relaxation to acetylcholine in SLE mice up to similar levels found in control mice. Probiotic treatment inhibited the up-regulation of NOX subunits and its activity in SLE mice. All the results suggest that the reduction of ROS levels in the vascular wall, and the subsequent prevention of NO inactivation, constitute a pivotal mechanism involved in the LC40 protective effects on endothelial function in SLE disease. Increased ROS production has also been involved in the rise of BP in female NZBWF1 mice because chronic treatment with a mixture of antioxidants decreased BP (25).

Another remarkable event involved in BP regulation is the T cells' infiltration in vascular tissues (62). In fact, preventing T-cell polarization in mesenteric lymph nodes by LC40 administration reduced T_H17 accumulation in aorta and improved endothelial dysfunction. The proinflammatory cytokine IL-17 causes Rho-kinase-mediated endothelial dysfunction in the vascular wall by increasing the phosphorylation of the inhibitory eNOS residue Thr⁴⁹⁵ (46). In addition, IL-17 promotes ROS generation by NOX activation (63). We found lower IL-17 mRNA levels in aortas from the SLE-LC40 group compared to SLE group, associated to reduced Rho expression, Thr⁴⁹⁵ eNOS phosphorylation, and NOX activity, which might be involved in the protective effect of LC40 administration in endothelial dysfunction. However, we did not test if there is a mechanistic link between vascular IL-17 level and both transcriptional and function changes found in SLE mice in the vascular wall.

Furthermore, the immune system is intimately associated with TLR signals, which are involved in the pathogenesis of SLE (64). Our findings revealed that aortic mRNA levels of TLR-4 were higher in NZBWF1 mice compared with control mice. In the vasculature, the activation of TLR-4 by the bacterial products, such as LPS, results in increased NOX-dependent O₂⁻ production and inflammation (50). Probiotic administration reduced plasma LPS levels with a subsequent reduction in the mRNA levels of TLR-4 and, consequently, improved vascular oxidative stress and inflammation in SLE. Moreover,

inflammatory responses in the endothelium induced by circulating autoantibodies and other inflammatory mediators are known to contribute to the pathogenesis of endothelial dysfunction (60), and numerous studies have related the release of cytokines to the progression of SLE (65). Therefore, we found increased plasma levels of proinflammatory cytokines TNF- α , IFN- γ , IL-17a, and IL-21 in SLE mice. LC40 treatment decreased the number of T_H1 cells, as well as IFN- γ and IL-21 levels in plasma; therefore, their deleterious effects on vasculature were decreased. One important limitation of our study is that we have not followed the evolution of the immunologic, vascular, and BP improvements induced by LC40, and it is not clear whether vascular and immunologic benefits are secondary to decreased BP or are early events involved in BP control.

In summary, our study showed that LC40 treatment in SLE mice improves endothelium-dependent relaxation and reduces SBP. These protective effects seem to be associated, at least in part, with a decrease in the vascular oxidative stress by restoring the expression of NOX subunits to normal values as a result of lower plasma levels of autoantibodies, proinflammatory cytokines, and LPS. In addition, the reduced vascular T_H17 infiltration contributed to the vascular protective effects of LC40. The decrease in T_H17 population in mesenteric lymph nodes might be related to an increase in colonic IL-18 and an increased enrichment of *Bifidobacterium* in the microbiota. This bacterium is commonly considered a beneficial bacterial genus that plays a critical role in the maturation and regulation of the immune system. These results open new possibilities to the prevention of cardiovascular complications associated with SLE by the modulation of the gut microbiota through the administration of probiotics. However, caution should be taken when extrapolating these findings to humans because of the potential differences in the features of the animal and human gut microbiota. In fact, the relative abundance of *Lactobacillales* appears to be normal in SLE patients in remission (6), which might alter the possible applicability of the LC40 treatment to clinical practice in humans. Moreover, the composition of gut microbiota in a large population of hypertensive SLE patients is unknown. Overall, our study suggests that beneficial bacteria capable of improving gut barrier function and reducing endotoxemia might prevent vascular complications in SLE patients. [F]

ACKNOWLEDGMENTS

The authors thank Nutraceutical Translations (Granada, Spain) for English language editing of this manuscript. This work was supported by grants from the Comisión Interministerial de Ciencia y Tecnología, Ministerio de Economía y Competitividad (MINECO) (SAF2014-55523-R, AGL2015-67995-C3-3-R, SAF2017-84894-R), Junta de Andalucía (Proyecto de excelencia P12-CTS-2722, AGR-6826, and CTS 164) with funds from the European Union, and by the Ministerio de Economía y Competitividad, Instituto de Salud Carlos III (CIBER-eht, CIBER-CV). M.S. is a postdoctoral fellow of Junta de Andalucía, I.R.-V. is a predoctoral fellow of MINECO, M.R. is postdoctoral fellow of the University of Granada, and N.D.L.V. is a predoctoral fellow of Junta de Andalucía and Fondo Social Europeo. "FEDER una manera de hacer Europa." The authors declare no conflicts of interest.

AUTHOR CONTRIBUTIONS

M. Toral, I. Robles-Vera, M. Romera, N. de la Visitación, M. Sánchez, F. O'Valle, A. Rodríguez-Nogales, and R. Jiménez, performed the experiments; M. Toral, M. Romero, F. O'Valle, A. Rodríguez-Nogales, J. Gálvez, J. Duarte, and R. Jiménez contributed to data analysis; M. Toral and J. Duarte participated in the research design and wrote or contributed to the writing of the manuscript; and all authors approved the final version to be published.

REFERENCES

1. Frostgård, J. (2008) Systemic lupus erythematosus and cardiovascular disease. *Lupus* **17**, 364–367
2. Bartels, C. M., Buhr, K. A., Goldberg, J. W., Bell, C. L., Visekruna, M., Nekkanti, S., and Greenlee, R. T. (2014) Mortality and cardiovascular burden of systemic lupus erythematosus in a US population-based cohort. *J. Rheumatol.* **41**, 680–687
3. Al-Herz, A., Ensworth, S., Shojania, K., and Esdaile, J. M. (2003) Cardiovascular risk factor screening in systemic lupus erythematosus. *J. Rheumatol.* **30**, 493–496
4. Ryan, M. J. (2009) The pathophysiology of hypertension in systemic lupus erythematosus. *Am. J. Physiol. Regul. Integr. Comp. Physiol.* **296**, R1258–R1267
5. Wu, J., Saleh, M. A., Kirabo, A., Itani, H. A., Montaniel, K. R., Xiao, L., Chen, W., Mernaugh, R. L., Cai, H., Bernstein, K. E., Goronzy, J. J., Weyand, C. M., Curci, J. A., Barbaro, N. R., Moreno, H., Davies, S. S., Roberts II, L. J., Madhur, M. S., and Harrison, D. G. (2016) Immune activation caused by vascular oxidation promotes fibrosis and hypertension. *J. Clin. Invest.* **126**, 1607; erratum: 50–67
6. Hevia, A., Milani, C., López, P., Cuervo, A., Arbolea, S., Duranti, S., Turroni, F., González, S., Suárez, A., Gueimonde, M., Ventura, M., Sánchez, B., and Margolles, A. (2014) Intestinal dysbiosis associated with systemic lupus erythematosus. *MBio* **5**, e01548-14
7. López, P., Sánchez, B., Margolles, A., and Suárez, A. (2016) Intestinal dysbiosis in systemic lupus erythematosus: cause or consequence? *Curr. Opin. Rheumatol.* **28**, 515–522
8. Luo, X. M., Edwards, M. R., Mu, Q., Yu, Y., Vieson, M. D., Reilly, C. M., Ahmed, S. A., and Bankole, A. A. (2018) Gut microbiota in human systemic lupus erythematosus and a mouse model of lupus. *Appl. Environ. Microbiol.* **84**, e02288-17
9. Zhang, H., Liao, X., Sparks, J. B., and Luo, X. M. (2014) Dynamics of gut microbiota in autoimmune lupus. *Appl. Environ. Microbiol.* **80**, 7551–7560
10. Mu, Q., Zhang, H., Liao, X., Lin, K., Liu, H., Edwards, M. R., Ahmed, S. A., Yuan, R., Li, L., Cecere, T. E., Branson, D. B., Kirby, J. L., Goswami, P., Leeth, C. M., Read, K. A., Oestreich, K. J., Vieson, M. D., Reilly, C. M., and Luo, X. M. (2017) Control of lupus nephritis by changes of gut microbiota. *Microbiome* **5**, 73
11. Mu, Q., Tavella, V. J., Kirby, J. L., Cecere, T. E., Chung, M., Lee, J., Li, S., Ahmed, S. A., Eden, K., Allen, I. C., Reilly, C. M., and Luo, X. M. (2017) Antibiotics ameliorate lupus-like symptoms in mice. *Sci. Rep.* **7**, 13675
12. Mardani, F., Mahmoudi, M., Esmaceli, S. A., Khorasani, S., Tabasi, N., and Rastin, M. (2018) In vivo study: Th1-Th17 reduction in pristane-induced systemic lupus erythematosus mice after treatment with tolerogenic Lactobacillus probiotics. *J. Cell. Physiol.* **234**, 642–649
13. Rudofsky, U. H., Dilwith, R. L., Roths, J. B., Lawrence, D. A., Kelley, V. E., and Magro, A. M. (1984) Differences in the occurrence of hypertension among (NZB X NZW)F1, MRL-lpr, and BXSb mice with lupus nephritis. *Am. J. Pathol.* **116**, 107–114
14. Small, H. Y., Migliarino, S., Czesnikiewicz-Guzik, M., and Guzik, T. J. (2018) Hypertension: focus on autoimmunity and oxidative stress. *Free Radic. Biol. Med.* **125**, 104–115
15. Ryan, M. J., and McLemore, G. R., Jr. (2007) Hypertension and impaired vascular function in a female mouse model of systemic lupus erythematosus. *Am. J. Physiol. Regul. Integr. Comp. Physiol.* **292**, R736–R742
16. Romero, M., Toral, M., Robles-Vera, I., Sánchez, M., Jiménez, R., O'Valle, F., Rodríguez-Nogales, A., Pérez-Vizcaino, F., Gálvez, J., and Duarte, J. (2017) Activation of peroxisome proliferator activator receptor β/δ improves endothelial dysfunction and protects kidney in murine lupus. *Hypertension* **69**, 641–650
17. McMurray, R. W., Hoffman, R. W., Nelson, W., and Walker, S. E. (1997) Cytokine mRNA expression in the B/W mouse model of systemic lupus erythematosus—analyses of strain, gender, and age effects. *Clin. Immunol. Immunopathol.* **84**, 260–268
18. Tzang, B. S., Liu, C. H., Hsu, K. C., Chen, Y. H., Huang, C. Y., and Hsu, T. C. (2017) Effects of oral Lactobacillus administration on antioxidant activities and CD4+CD25+forkhead box P3 (FoxP3)+ T cells in NZB/W F1 mice. *Br. J. Nutr.* **118**, 333–342
19. Martín, B. S., Langa, S., Reviriego, C., Jiménez, E., Marín, M. L., Xaus, J., Fernández, L., and Rodríguez, J. M. (2003) Human milk is a source of lactic acid bacteria for the infant gut. *J. Pediatr.* **143**, 754–758
20. Martín, R., Olivares, M., Marín, M. L., Fernández, L., Xaus, J., and Rodríguez, J. M. (2005) Probiotic potential of 3 Lactobacilli strains isolated from breast milk. *J. Hum. Lact.* **21**, 8–17; quiz 18–21, 41
21. Gómez-Guzmán, M., Toral, M., Romero, M., Jiménez, R., Galindo, P., Sánchez, M., Zarzuelo, M. J., Olivares, M., Gálvez, J., and Duarte, J. (2015) Antihypertensive effects of probiotics Lactobacillus strains in spontaneously hypertensive rats. *Mol. Nutr. Food Res.* **59**, 2326–2336
22. Toral, M., Romero, M., Rodríguez-Nogales, A., Jiménez, R., Robles-Vera, I., Algieri, F., Chueca-Porcuna, N., Sánchez, M., de la Visitación, N., Olivares, M., García, F., Pérez-Vizcaino, F., Gálvez, J., and Duarte, J. (2018) Lactobacillus fermentum improves tacrolimus-induced hypertension by restoring vascular redox state and improving eNOS coupling. *Mol. Nutr. Food Res.* **30**, e1800033
23. Robles-Vera, I., Toral, M., de la Visitación, N., Sánchez, M., Romero, M., Olivares, M., Jiménez, R., and Duarte, J. (2018) The probiotic Lactobacillus fermentum prevents dysbiosis and vascular oxidative stress in rats with hypertension induced by chronic nitric oxide blockade. *Mol. Nutr. Food Res.* **62**, e1800298
24. Toral, M., Gómez-Guzmán, M., Jiménez, R., Romero, M., Sánchez, M., Utrilla, M. P., Garrido-Mesa, N., Rodríguez-Cabezas, M. E., Olivares, M., Gálvez, J., and Duarte, J. (2014) The probiotic Lactobacillus coryniformis CECT5711 reduces the vascular pro-oxidant and pro-inflammatory status in obese mice. *Clin. Sci. (Lond.)* **127**, 33–45
25. Gómez-Guzmán, M., Jiménez, R., Romero, M., Sánchez, M., Zarzuelo, M. J., Gómez-Morales, M., O'Valle, F., López-Farré, A. J., Algieri, F., Gálvez, J., Pérez-Vizcaino, F., Sabio, J. M., and Duarte, J. (2014) Chronic hydroxychloroquine improves endothelial dysfunction and protects kidney in a mouse model of systemic lupus erythematosus. *Hypertension* **64**, 330–337
26. Venegas-Pont, M., Sartori-Valinotti, J. C., Maric, C., Racusen, L. C., Glover, P. H., McLemore, G. R., Jr., Jones, A. V., Reckelhoff, J. F., and Ryan, M. J. (2009) Rosiglitazone decreases blood pressure and renal injury in a female mouse model of systemic lupus erythematosus. *Am. J. Physiol. Regul. Integr. Comp. Physiol.* **296**, R1282–R1289
27. Haarman, M., and Knol, J. (2006) Quantitative real-time PCR analysis of fecal Lactobacillus species in infants receiving a prebiotic infant formula. *Appl. Environ. Microbiol.* **72**, 2359–2365
28. Heilig, H. G., Zoetendal, E. G., Vaughan, E. E., Marteau, P., Akkermans, A. D., and de Vos, W. M. (2002) Molecular diversity of Lactobacillus spp. and other lactic acid bacteria in the human intestine as determined by specific amplification of 16S ribosomal DNA. *Appl. Environ. Microbiol.* **68**, 114–123
29. Gil-Campos, M., López, M. Á., Rodríguez-Benítez, M. V., Romero, J., Roncero, I., Linares, M. D., Maldonado, J., López-Huertas, E., Berwind, R., Ritzenthaler, K. L., Navas, V., Sierra, C., Sempere, L., Geerlings, A., Maldonado-Lobón, J. A., Valero, A. D., Lara-Villoslada, F., and Olivares, M. (2012) Lactobacillus fermentum CECT 5716 is safe and well tolerated in infants of 1-6 months of age: a randomized controlled trial. *Pharmacol. Res.* **65**, 231–238
30. Dole, V. S., Henderson, K. S., Fister, R. D., Pietrowski, M. T., Maldonado, G., and Clifford, C. B. (2013) Pathogenicity and genetic variation of 3 strains of *Corynebacterium bovis* in immunodeficient mice. *J. Am. Assoc. Lab. Anim. Sci.* **52**, 458–466
31. Caporaso, J. G., Lauber, C. L., Walters, W. A., Berg-Lyons, D., Lozupone, C. A., Turnbaugh, P. J., Fierer, N., and Knight, R. (2011) Global patterns of 16S rRNA diversity at a depth of millions of sequences per sample. *Proc. Natl. Acad. Sci. USA* **108**(Suppl 1), 4516–4522
32. Zhou, H. W., Li, D. F., Tam, N. F., Jiang, X. T., Zhang, H., Sheng, H. F., Qin, J., Liu, X., and Zou, F. (2011) BIPES, a cost-effective high-throughput method for assessing microbial diversity. *ISME J.* **5**, 741–749
33. Liu, Z., Liu, H. Y., Zhou, H., Zhan, Q., Lai, W., Zeng, Q., Ren, H., and Xu, D. (2017) Moderate-intensity exercise affects gut microbiome

- composition and influences cardiac function in myocardial infarction mice. *Front. Microbiol.* **8**, 1687
34. Edgar, R. C., and Flyvbjerg, H. (2015) Error filtering, pair assembly and error correction for next-generation sequencing reads. *Bioinformatics* **31**, 3476–3482
 35. Wang, Q., Garrity, G. M., Tiedje, J. M., and Cole, J. R. (2007) Naive Bayesian classifier for rapid assignment of rRNA sequences into the new bacterial taxonomy. *Appl. Environ. Microbiol.* **73**, 5261–5267
 36. Antharam, V. C., Li, E. C., Ishmael, A., Sharma, A., Mai, V., Rand, K. H., and Wang, G. P. (2013) Intestinal dysbiosis and depletion of butyrogenic bacteria in Clostridium difficile infection and nosocomial diarrhea. *J. Clin. Microbiol.* **51**, 2884–2892
 37. Segata, N., Izard, J., Waldron, L., Gevers, D., Miropolsky, L., Garrett, W. S., and Huttenhower, C. (2011) Metagenomic biomarker discovery and explanation. *Genome Biol.* **12**, R60
 38. Yang, T., Santisteban, M. M., Rodriguez, V., Li, E., Ahmari, N., Carvajal, J. M., Zadeh, M., Gong, M., Qi, Y., Zubcevic, J., Sahay, B., Pepine, C. J., Raizada, M. K., and Mohamadzadeh, M. (2015) Gut dysbiosis is linked to hypertension. *Hypertension* **65**, 1331–1340
 39. Zuo, L., Yuan, K. T., Yu, L., Meng, Q. H., Chung, P. C., and Yang, D. H. (2014) Bifidobacterium infantis attenuates colitis by regulating T cell subset responses. *World J. Gastroenterol.* **20**, 18316–18329
 40. Hsieh, C. Y., Osaka, T., Moriyama, E., Date, Y., Kikuchi, J., and Tsuneda, S. (2015) Strengthening of the intestinal epithelial tight junction by Bifidobacterium bifidum. *Physiol. Rep.* **3**, e12327
 41. Elinav, E., Henao-Mejia, J., and Flavell, R. A. (2013) Integrative inflammasome activity in the regulation of intestinal mucosal immune responses. *Mucosal Immunol.* **6**, 4–13
 42. Harrison, O. J., Srinivasan, N., Pott, J., Schiering, C., Krausgruber, T., Ilott, N. E., and Maloy, K. J. (2015) Epithelial-derived IL-18 regulates Th17 cell differentiation and Foxp3⁺ Treg cell function in the intestine. *Mucosal Immunol.* **8**, 1226–1236
 43. Geddes, K., and Philpott, D. J. (2008) A new role for intestinal alkaline phosphatase in gut barrier maintenance. *Gastroenterology* **135**, 8–12
 44. Bates, J. M., Akerlund, J., Mitge, E., and Guillemin, K. (2007) Intestinal alkaline phosphatase detoxifies lipopolysaccharide and prevents inflammation in zebrafish in response to the gut microbiota. *Cell Host Microbe* **2**, 371–382
 45. Wofsy, D., Chiang, N. Y., Greenspan, J. S., and Ermak, T. H. (1988) Treatment of murine lupus with monoclonal antibody to L3T4. I. Effects on the distribution and function of lymphocyte subsets and on the histopathology of autoimmune disease. *J. Autoimmun.* **1**, 415–431
 46. Talaat, R. M., Mohamed, S. F., Bassyouni, I. H., and Raouf, A. A. (2015) Th1/Th2/Th17/Treg cytokine imbalance in systemic lupus erythematosus (SLE) patients: correlation with disease activity. *Cytokine* **72**, 146–153
 47. Dar, O., Salaman, M. R., Seifert, M. H., and Isenberg, D. A. (1988) B lymphocyte activation in systemic lupus erythematosus: spontaneous production of IgG antibodies to DNA and environmental antigens in cultures of blood mononuclear cells. *Clin. Exp. Immunol.* **73**, 430–435
 48. Nguyen, H., Chiasson, V. L., Chatterjee, P., Kopriva, S. E., Young, K. J., and Mitchell, B. M. (2013) Interleukin-17 causes Rho-kinase-mediated endothelial dysfunction and hypertension. *Cardiovasc. Res.* **97**, 696–704
 49. Kim, F., Tysseling, K. A., Rice, J., Pham, M., Haji, L., Gallis, B. M., Baas, A. S., Paramsothy, P., Giachelli, C. M., Corson, M. A., and Raines, E. W. (2005) Free fatty acid impairment of nitric oxide production in endothelial cells is mediated by IKKbeta. *Arterioscler. Thromb. Vasc. Biol.* **25**, 989–994
 50. Liang, C. F., Liu, J. T., Wang, Y., Xu, A., and Vanhoutte, P. M. (2013) Toll-like receptor 4 mutation protects obese mice against endothelial dysfunction by decreasing NADPH oxidase isoforms 1 and 4. *Arterioscler. Thromb. Vasc. Biol.* **33**, 777–784
 51. Cavallo, T., and Granholm, N. A. (1990) Bacterial lipopolysaccharide transforms mesangial into proliferative lupus nephritis without interfering with processing of pathogenic immune complexes in NZB/W mice. *Am. J. Pathol.* **137**, 971–978
 52. Granholm, N. A., and Cavallo, T. (1994) Long-lasting effects of bacterial lipopolysaccharide promote progression of lupus nephritis in NZB/W mice. *Lupus* **3**, 507–514
 53. Mack, D. R., Michail, S., Wei, S., McDougall, L., and Hollingsworth, M. A. (1999) Probiotics inhibit enteropathogenic E. coli adherence in vitro by inducing intestinal mucin gene expression. *Am. J. Physiol.* **276**, G941–G950
 54. Kaliannan, K., Wang, B., Li, X. Y., Kim, K. J., and Kang, J. X. (2015) A host-microbiome interaction mediates the opposing effects of omega-6 and omega-3 fatty acids on metabolic endotoxemia. *Sci. Rep.* **5**, 11276
 55. Spolski, R., and Leonard, W. J. (2014) Interleukin-21: a double-edged sword with therapeutic potential. *Nat. Rev. Drug Discov.* **13**, 379–395
 56. Lauwerys, B. R., Renaud, J. C., and Houssiau, F. A. (1998) Inhibition of in vitro immunoglobulin production by IL-12 in murine chronic graft-vs.-host disease: synergism with IL-18. *Eur. J. Immunol.* **28**, 2017–2024
 57. Zhang, M., Yu, G., Chan, B., Pearson, J. T., Rathanaswami, P., Delaney, J., Ching Lim, A., Babcock, J., Hsu, H., and Gavin, M. A. (2015) Interleukin-21 receptor blockade inhibits secondary humoral responses and halts the progression of preestablished disease in the (NZB × NZW)F1 systemic lupus erythematosus model. *Arthritis Rheumatol.* **67**, 2723–2731
 58. Mathis, K. W., Wallace, K., Flynn, E. R., Maric-Bilkan, C., LaMarca, B., and Ryan, M. J. (2014) Preventing autoimmunity protects against the development of hypertension and renal injury. *Hypertension* **64**, 792–800
 59. Alunno, A., Bartoloni, E., Bistoni, O., Nocentini, G., Ronchetti, S., Caterbi, S., Valentini, V., Riccardi, C., and Gerli, R. (2012) Balance between regulatory T and Th17 cells in systemic lupus erythematosus: the old and the new. *Clin. Dev. Immunol.* **2012**, 823085
 60. Toral, M., Jiménez, R., Romero, M., Robles-Vera, I., Sánchez, M., Salaces, M., Sabio, J. M., and Duarte, J. (2017) Role of endoplasmic reticulum stress in the protective effects of PPARβ/δ activation on endothelial dysfunction induced by plasma from patients with lupus. *Arthritis Res. Ther.* **19**, 268
 61. Tschudi, M. R., Barton, M., Bersinger, N. A., Moreau, P., Cosentino, F., Noll, G., Malinski, T., and Lüscher, T. F. (1996) Effect of age on kinetics of nitric oxide release in rat aorta and pulmonary artery. *J. Clin. Invest.* **98**, 899–905
 62. Ryan, M. J. (2013) An update on immune system activation in the pathogenesis of hypertension. *Hypertension* **62**, 226–230
 63. Dhillion, P., Wallace, K., Herse, F., Scott, J., Wallukat, G., Heath, J., Mosely, J., Martin, J. N., Jr., Dechend, R., and LaMarca, B. (2012) IL-17-mediated oxidative stress is an important stimulator of AT1-AA and hypertension during pregnancy. *Am. J. Physiol. Regul. Integr. Comp. Physiol.* **303**, R353–R358
 64. Ma, K., Li, J., Fang, Y., and Lu, L. (2015) Roles of B cell-intrinsic TLR signals in systemic lupus erythematosus. *Int. J. Mol. Sci.* **16**, 13084–13105
 65. Kelley, V. R., and Wüthrich, R. P. (1999) Cytokines in the pathogenesis of systemic lupus erythematosus. *Semin. Nephrol.* **19**, 57–66

Received for publication February 26, 2019.

Accepted for publication May 7, 2019.